CHARACTERIZATION OF CHINESE HYDROTHERMAL SYNTHETIC EMERALD

By Karl Schmetzer, Lore Kiefert, Heinz-Jürgen Bernhardt, and Zhang Beili

Synthetic emeralds grown hydrothermally in an alkali-free, chlorine-bearing solution have been manufactured in Guilin, China, since 1987. Diagnostic microscopic features include growth and color zoning as well as oriented needle-like tubes and cone-shaped voids ("nailhead spicules") that are typically associated with small chrysoberyl crystals. Also distinctive is the presence of chlorine in this iron- and alkali-free hydrothermal synthetic emerald. In addition, spectroscopic properties in the mid- and near-infrared are useful to characterize this new Chinese product; features in the 2500–3100 cm^{-1} range (also found in other chlorine-bearing synthetic emeralds) help distinguish it from natural emeralds.

ABOUT THE AUTHORS

Dr. Schmetzer is a research scientist residing in Petershausen, near Munich, Germany. Dr. Kiefert is a research scientist at the SSEF Swiss Gemmological Institute, Basel, Switzerland. Dr. Bernhardt is a research scientist at the Institute of Mineralogy of Ruhr University, Bochum, Germany. Professor Zhang is director of the National Gemstone Testing Center, Beijing, China.

Please see acknowledgments at end of article.

Gems & Gemology, *Vol. 33, No. 4, pp. 276–291*

© 1997 Gemological Institute of America

During a visit to Beijing in May 1996, one of the authors (KS) was shown several rough and faceted samples of a hydrothermal synthetic emerald that was manufactured in China (see, e.g., figure 1). This synthetic emerald has been produced since 1987 by Professor Zeng Jiliang at the Institute of Geology for Mineral Resources, CNNC, Guilin, Guangxi Province, southern China. It was first commercially released in 1993. At present, production is about 7,500 ct of rough a year, but this amount is expected to increase (Guo Tao, pers. comm., 1996, 1997). Samples have been sold under different trade names (Fritsch, 1996; C. M. Ou-Yang, pers. comm., 1997), but at present only "GJL-Emerald" (Guangxi Jewellery Limited) is used by the manufacturers (C. M. Ou-Yang, pers. comm., 1997).

Hydrothermally grown synthetic emeralds have been commercially available since the early 1960s. They were first produced in Austria (Lechleitner) and later in the United States (Linde, Regency), Australia (Biron), and Russia (Pough, 1965; Flanigen et al., 1965, 1967; Galia, 1972; Nassau, 1976; Brown and Snow, 1984; Kane and Liddicoat, 1985; Bukin et al., 1986; Schmetzer, 1988, 1990; Hosaka, 1990; Koivula et al., 1996). Hydrothermally grown synthetic emeralds from China were first described by Geng and Ou-Yang (1995). They were also briefly mentioned by Fritsch (1996) and Koivula et al. (1996), but to date there has been no comprehensive gemological description of this material.

This article reports on our examination of several crystals and faceted samples of this Chinese hydrothermal synthetic emerald. To help establish criteria by which they can be separated from their natural counterparts, we will describe in detail the mineralogical, gemological, chemical, and spectroscopic characteristics of these new synthetic gems. We will also compare these properties to those of various synthetic

Figure 1. This 4.72 ct crystal (sample H) and the 0.13–0.61 ct faceted samples are some of the hydrothermal synthetic emeralds grown in China that were examined for this study. The wires used to suspend the seed are visible on both ends of the crystal. Photo © GIA and Tino Hammid.

emeralds that have been hydrothermally grown by other commercial producers.

BACKGROUND ON CRYSTAL GROWTH

According to their producer, these Chinese synthetic emeralds are grown in autoclaves with gold liners at a temperature range of 585°–625°C and a pressure of 4.50 kbar (Guo Tao, pers. comm., 1996, 1997). This pressure is much higher than that normally used for the commercial growth of hydrothermal synthetic emeralds—that is, 0.70 to 1.53 kbar, as summarized by Hosaka (1990)—but in a similar temperature range of 500°–620°C. Therefore, the Chinese hydrothermal synthetic emeralds may be the first that are commercially produced at a pressure above 2 kbar.

The high-pressure synthesis of beryl was described by Franz and Morteani (1981) at 2 kbar and a temperature of 700°C as well as at 4 kbar and 500°C. Kodaira et al. (1982) synthesized beryl at an even higher pressure of 10 kbar, at 650°C to 750°C. They obtained prismatic crystals up to 0.3 mm in length.

The Chinese material grows at about 0.5 mm a day in a direction perpendicular to the seed plate. Both natural and synthetic beryl seed plates are used (Fritsch, 1996; Guo Tao and C. M. Ou-Yang, pers. comm., 1997). The producer also stated that he has grown two types of hydrothermal synthetic emerald: one with only chromium used as a color-causing dopant, and the second with chromium, vanadium, and iron compounds in the nutrient

and/or in the solution (Geng and Ou-Yang, 1995). Only the first type is now produced commercially (Guo Tao, pers. comm., 1997).

MATERIALS AND METHODS

For this study, we examined 11 Chinese hydrothermal synthetic emeralds (see table 1): a 12.12 ct crystal (sample A) that was acquired in China from the producer in 1994 by Prof. H. A. Hänni; a 7.40 ct crystal (sample B) and five faceted "stones" (0.31 to 0.50 ct; samples C to G) that the producer made available for the present investigation in 1996; and a 4.72 ct crystal (sample H) and three faceted pieces (0.13 to 0.61 ct; samples I to K) from the GIA Research collection that were obtained from the producer in 1995 by Prof. E. Fritsch.

All 11 samples (most of which are shown in figure 1) were tested by standard gemological methods for optical properties, fluorescence, and specific gravity. Morphological characteristics of the three crystals were determined with a standard goniometer, and the external faces of these crystals as well as the internal growth planes of all 11 samples were examined with a Schneider horizontal (immersion) microscope with a specially designed sample holder and specially designed (to measure angles) eyepieces (Schmetzer, 1986; Kiefert and Schmetzer, 1991). Solid inclusions were identified by Raman spectroscopy with a Renishaw Raman microscope (see Hänni et al., 1996, 1997).

For chemical characterization, we first submitted samples A to G for qualitative energy-dispersive X-ray fluorescence (EDXRF) analysis using a Spectrace 5000 Tracor X-ray fluorescence spectrometer with a Tracor Northern Spectrace TX-6100 software system, at SSEF. Quantitative chemical data for Cr, V, and Fe in crystal samples A and B were determined with the same equipment. The quantitative chemical compositions of faceted samples C to G were determined by electron microprobe using a CAMECA Camebax SX 50 instrument, with traverses of 100 point analyses measured across the table of each sample.

For samples A to G, spectroscopic data were recorded with a Leitz-Unicam SP 800 spectrophotometer for the visible and ultraviolet range, and with a Hitachi U 4001 instrument for the UV, visible, and near-infrared range (from 250 to 2500 nm). Infrared spectroscopy for the range 6000 cm^{-1} to 1000 cm^{-1} was performed for the same seven samples on a Philips PU 9800 Fourier-transform infrared (FTIR) spectrometer and a Perkin-Elmer 1760 FTIR spectrometer.

Faceted sample F was cut in two pieces, and one of these pieces was powdered. We used 2 mg of the powder to prepare a KBr compressed disk for infrared spectroscopy in the 4000–2000 cm^{-1} range

TABLE 1. Physical characteristics of Chinese hydrothermal synthetic emerald samples.

Sample	A	B	C	D	E	F	G	H	I[b]	J	K[b]
Description	Crystal	Crystal	Faceted	Faceted	Faceted	Faceted	Faceted	Crystal	Faceted	Faceted	Faceted
Weight (ct)	12.12	7.40	0.50	0.39	0.43	0.41	0.31	4.72	0.13	0.22	0.61
Seed type	Natural colorless beryl	Natural colorless beryl	Synthetic emerald	Not observed	Natural colorless beryl	Synthetic emerald	Not observed	Synthetic emerald	Synthetic emerald	Synthetic emerald	Synthetic emerald
Seed inclination to c-axis	20°	33°	34°	32° bent plane	38°	40°	Not observed	20°	33°	35°	36°, 44° bent plane
Microscopic features[a]	Planar color zoning, irreg. subgrain bounds., small feathers	Planar color zoning, irreg. subgrain bounds., single cones w/ beryl xls, small feathers	Planar color zoning, numerous cones w/ chrysoberyl xls, needles at growth plane, small feathers	Planar color zoning, irreg. subgrain bounds., needles at growth plane	Planar color zoning, single cones w/ beryl xls, numerous cones w/ chrysoberyl xls	Planar color zoning, numerous cones w/ chrysoberyl xls, needles in seed	Irregular color zoning, prominent irreg. subgrain bounds.	Planar color zoning, irreg. subgrain bounds., large feathers	Planar color zoning, irreg. subgrain bounds., numerous cones w/ xls, needles at growth plane	Planar color zoning, irreg. subgrain bounds., numerous cones w/ chrysoberyl xls, needles in seed	Planar color zoning, irreg. subgrain bounds., numerous cones w/ xls

[a]*Cones = cone-shaped fluid inclusions; irreg. subgrain bounds. = irregular subgrain boundaries; xls = crystals (minerals identified by Raman spectroscopy); needles = needle-like tubes*
[b]*In these two samples, the tiny crystals were optically identical to the chrysoberyl crystals identified by Raman spectroscopy in other samples.*

using a Nicolet-Impact 400D infrared spectrometer. The remaining 38 mg of powder was used for the quantitative determination of Li_2O and H_2O by wet chemical methods.

For comparison purposes, two of the authors (KS and LK) drew on infrared and EDXRF data gathered for other hydrothermal synthetic emeralds. The senior author (KS) has also examined the microscopic features of about 100 hydrothermal synthetic emeralds from different producers. From these samples, he selected 20 for Raman spectroscopy of nailhead spicules (Linde and Regency, 6; Biron, Pool, and AGEE, 5; and Lechleitner, 9), which was conducted as described above for the Chinese samples. Note that the Lechleitner samples included both the synthetic emerald overgrowth over natural beryl and fully synthetic emeralds. Unless otherwise noted, all references to Lechleitner in this article will refer to both products.

RESULTS

Visual Appearance and Crystallography. When examined with the unaided eye, all the samples appeared an intense, homogeneous green without any prominent color zoning (again, see figure 1). A colorless seed plate was easily seen in crystal samples A and B, and the surface of each had residues of the metallic wire used to hold the seed. Careful examination of crystal sample H showed a green seed. On one end of this seed, residue of a metallic wire was overgrown by synthetic emerald. At the other end of the crystal, a second metallic wire traversed both the seed and the synthetic emerald overgrowth (see figure 1).

All three Chinese crystals showed the basal pinacoid *c* (0001), two prism faces, *m* ($10\bar{1}0$) and *a* ($11\bar{2}0$), as well as the hexagonal dipyramid *p* ($10\bar{1}2$) (figure 2). In all cases, the seeds were oriented as drawn in figure 3, that is, with angles of 20° or 33° between the seed and the c-axis (optic axis). Only sample A showed the two large uneven faces parallel to the seed (figures 3 and 4) that are commonly observed in hydrothermally grown synthetic emeralds (see Pough, 1965; Lebedev et al., 1986; Hosaka, 1990; Sosso and Piacenza, 1995; Sechos, 1997). Because their seeds had different length-to-width ratios, sample H had only one small face parallel to the seed and sample B had none with that orientation (figure 3).

All three crystals were strongly distorted; that is, the two *a* ($11\bar{2}0$) prism faces in the *a*–*c* seed zone

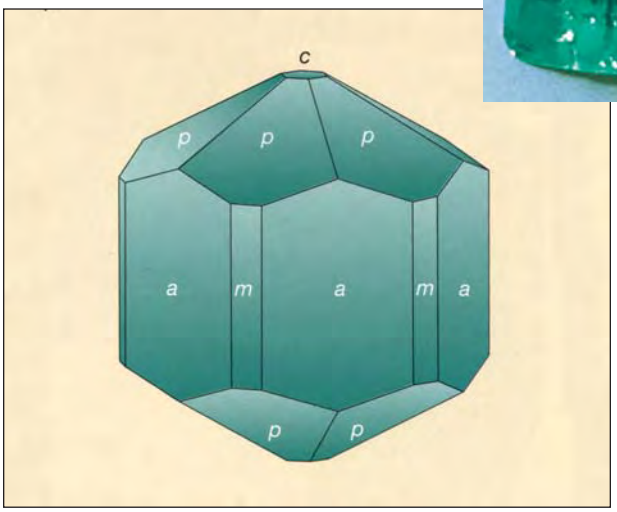

Figure 2. All three crystals of Chninese of Chinese hydrothermal synthetic emerald (see, e.g., 7.40 ct sample B in the inset photo) showed the basal pinacoid c, *first-and second-order hexagonal prisms* m *and* a, *and the hexagonal dipyramid* p, *as illustrated in this schematic drawing of an undistorted crystal. Photo by H. A. Hänni*

were dominant, and the four symmetrically equivalent *a* prism faces were distinctly smaller or absent. In addition, on each side, only two of six possible *p* dipyramids were developed (see figure 3).

Gemological Properties. The gemological properties of our Chinese samples (table 2) overlap those of natural emeralds, especially low-alkali emeralds, from various localities (see, e.g., Schrader, 1983). They are in the range commonly observed for low-iron or iron-free hydrothermally grown synthetic emeralds (see references cited above). Specifically, the values for R.I. and S.G. are similar to those observed for Lechleitner, Linde, Regency, and Biron synthetic emeralds, but they are distinctly lower than those of both types of (high-iron) Russian hydrothermal synthetic emeralds. The moderate fluorescence to UV radiation also indicates the absence of significant iron in the Chinese samples.

Microscopic Characteristics. *Structural Properties.* We observed seeds in six of the eight faceted Chinese samples (again, see table 1). The seed in sample E was colorless beryl (figure 5), similar to crystal samples A and B; as in those crystals (figure 6), the seed was of variable thickness. The other seeds were synthetic emerald, as in crystal sample

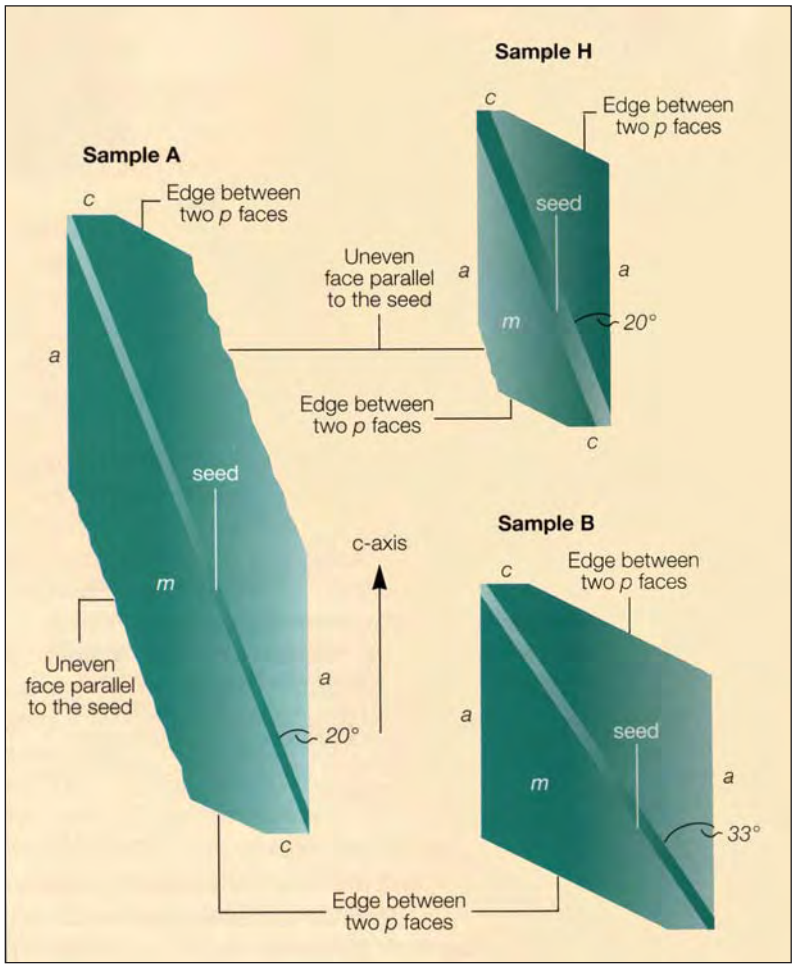

Figure 3. In this illustration (drawn to scale), Chinese hydrothermal synthetic crystal samples A, B, and H are shown as they appear when viewed parallel to the seed. The c-axis is parallel to the prism a *and perpendicular to the basal pinacoid* c*; the seeds are inclined to the c-axis at the angles indicated. Also shown is the edge at which the two* p *faces intersect. Two large uneven faces parallel to the seed are developed in sample A; only one uneven face was seen in sample H and none in sample B. The morphology of the crystals is related to the orientations and sizes of the seeds, which are (length × width × thickness) 21.5 × 8.0 × 0.4 mm in sample A, 13.5 × 11.0 × 0.15 mm in sample B, and 10.6 × 13.6 × 0.5 mm in sample H.*

H. In one of these faceted samples, the seed had a bent surface on one side (figure 7).

In all the Chinese samples found to contain seeds, we observed growth zoning, usually associated with color zoning, that was oriented parallel to the seed (figures 5, 6, and 8). In one sample without a seed, we saw bent zoning similar to that shown in figure 7. In some cases, the growth structures revealed a weak step-like microstructure (again, see figure 6), similar to that seen in various other hydrothermal synthetic emeralds (Galia, 1972; Lebedev and Askhabov, 1984; Schmetzer, 1988).

Figure 4. The face with this uneven, undulating surface was one of two oriented parallel to the seed in Chinese hydrothermal synthetic emerald sample A. Photo by H. A. Hänni; magnified 25×.

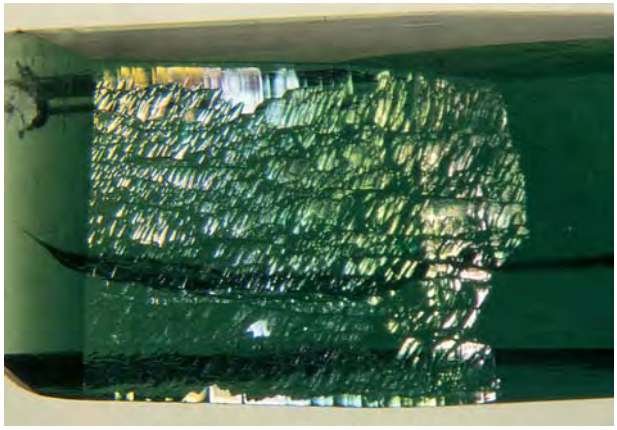

TABLE 2. Properties of 11 Chinese hydrothermal synthetic emeralds.

Color	Very slightly bluish green
Pleochroism	ω=yellowish green, ε=bluish green
Refractive indices	n_ω=1.576–1.578 n_ε=1.570–1.572
Birefringence	0.006
Specific gravity	Rough: 2.70–2.71 Faceted: 2.67–2.69
UV fluorescence	Short-wave: moderate red Long-wave: moderate red

Some of the samples revealed irregular boundaries between subindividuals (figure 9), occasionally in the form of an undulating, chevron-like growth pattern. This type of growth structure also is typical of other hydrothermal synthetic emeralds (Lebedev et al., 1986; Schmetzer, 1988; Henn et al., 1988; Hänni, 1993; Sechos, 1997). Note that this growth pattern was not seen in the two samples (E and F) in which the seed was inclined more than 35° to the c-axis, as was also the case for some Russian hydrothermal synthetic emeralds in which the seeds were at an angle of about 45° with the c-axis (Schmetzer, 1996).

Inclusions Related to the Seed or to Growth Planes. We commonly observed three types of elongated inclusions in the Chinese samples. These were related either to the seed or to growth planes in the synthetic emerald overgrowth; they were oriented either inclined to the seed or almost perpendicular to the seed, as illustrated in figure 10. In general, these inclusions appeared as one of two types of cone-shaped spicules (also called nailhead spicules when a crystalline "head" is present) or as needle-like tubes. All were filled with a fluid; some also had a gas bubble.

In the first type of spicule, which occurs as an isolated inclusion oriented parallel to the c-axis, the widest end of the cone is in direct contact with a tiny crystal at the seed; the narrower tip pointed in the direction of growth (figures 10A and 11). This general orientation has been described often in the gemological literature (Flanigen et al., 1967; Galia, 1972; Sunagwa, 1982; Hosaka, 1990). The tiny birefringent crystals have a refractive index close to that of the host emerald, so they can be difficult to observe without crossed polarizers.

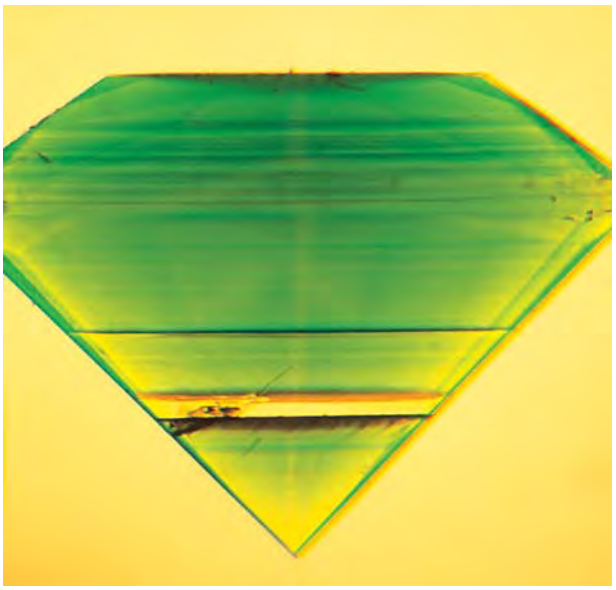

Figure 5. Faceted sample E has a colorless natural beryl seed that almost parallels the table facet, with growth zoning and color zoning parallel to the seed. Note that the seed appears yellow because the stone is immersed in benzyl benzoate. Magnified 35×.

Figure 6. Some of the colorless seeds in the Chinese synthetic emeralds examined were of variable thickness, as shown here in crystal sample B. Note also the step-like microstructures in the color zoning parallel to the seed, which resembles the irregular growth patterns seen in other hydrothermal synthetic emeralds. Immersion, magnified 50×.

Figure 7. One side of the synthetic emerald seed in faceted sample K is bent. Numerous tiny crystals can be seen throughout both sides of the synthetic seed, as well as cone-shaped spicules oriented parallel to the c-axis. Note also the distinct growth zoning in the seed itself. Immersion, magnified 40×.

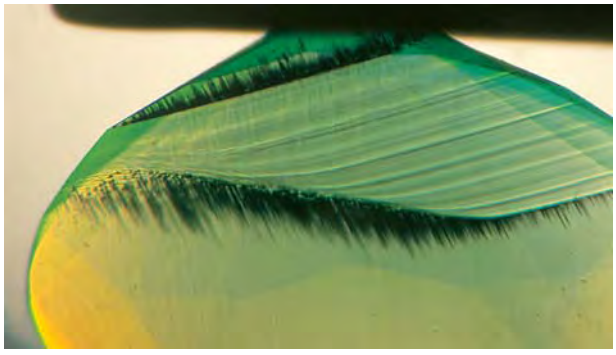

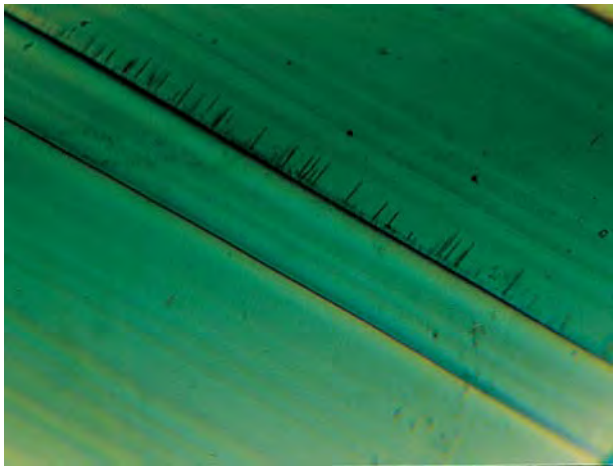

Figure 8. Growth planes, with associated color zoning, were seen oriented parallel to the seed in all of the Chinese samples that had seeds (upper right). Note also in this sample (C) the needle-like tubes that are elongated almost perpendicular to—and end at—one of the growth planes. Immersion, magnified 60×.

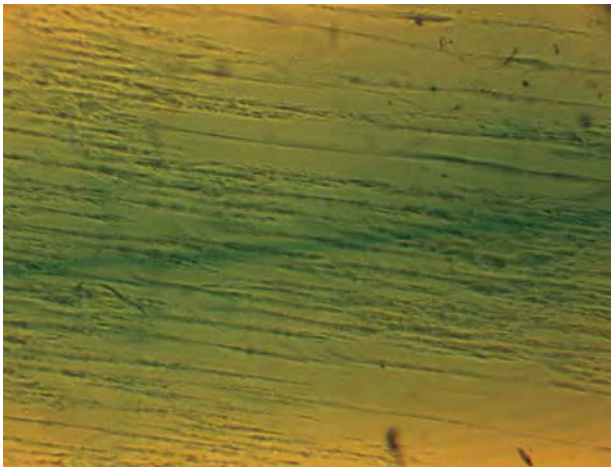

Figure 9. The growth structure of this Chinese hydrothermal synthetic emerald (sample G) revealed irregular boundaries between subindividuals. Immersion, magnified 60×.

The second type of spicule occurs in groups, also parallel to the c-axis, all with their widest ends at or very near the seed (figures 10 and 12). In direct contact with the seed are numerous small crystals (figure 13) that are also birefringent but have a refractive index that is distinctly higher than that of the host beryl.

The needle-like tubes are oriented almost perpendicular (measured at 80° to 85°) to the seed (fig-

Figure 10. This schematic drawing illustrates the different types of characteristic inclusions observed in the Chinese hydrothermal synthetic emeralds: (A) a colorless beryl seed with an isolated beryl crystal and numerous chrysoberyl crystals, both commonly associated with cone-shaped spicules (in all four inclusion types, these spicules parallel the c-axis); (B) a synthetic emerald seed with numerous chrysoberyl crystals—and cone-shaped spicules—on both sides; (C) a synthetic emerald seed with needle-like tubes within the seed (grown in the first autoclave run) and almost perpendicular to its surface, as well as with numerous chrysoberyl crystals on both sides of the seed; (D) a synthetic emerald seed with numerous chrysoberyl crystals and the cone-shaped spicules—a growth plane away from the seed reveals needle-like tubes with an orientation almost perpendicular to the growth plane that end at the growth plane.

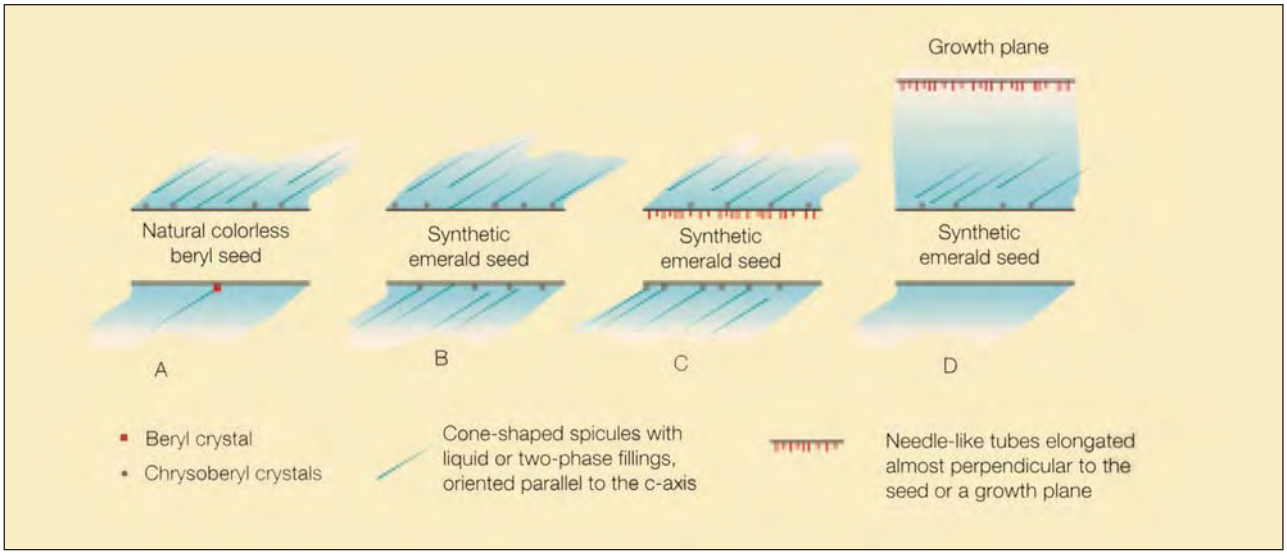

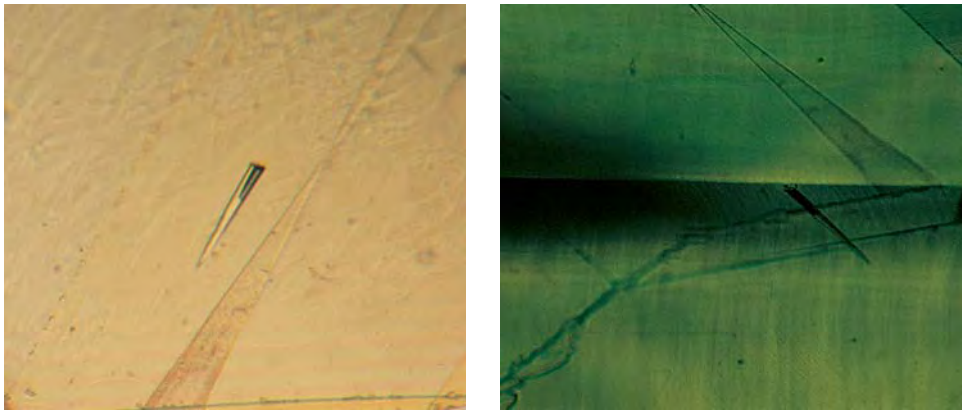

Figure 11. Occasionally seen in the Chinese hydrothermal synthetic emeralds examined were isolated cone-shaped spicules filled with a liquid or liquid and gas (left), and associated with a tiny crystal at their widest ends. The tiny crystal is in contact with the surface of the seed (right). Immersion, magnified 80×.

ures 10C and D, 14)—that is, inclined to the c-axis of the host. One end of the tube is always in direct contact with the seed or a growth plane parallel to the seed. In samples C, D, and I, there were no associated crystalline inclusions at the growth planes (again, see figure 8). In samples F and J, we observed these needle-like tubes *within* the seed, with cone-shaped spicules and birefringent crystals in the adjacent synthetic emerald overgrowth (again, see figure 14).

Other Liquid Inclusions. With the exception of the above-described inclusions, the samples were relatively clean. Only small liquid feathers were observed occasionally.

Figure 12. In the second type of elongated inclusion observed in the Chinese samples, numerous cone-shaped spicules with liquid or two-phase fillings, similar to the isolated inclusions shown in figure 11, also parallel the c-axis. These spicules start at the synthetic emerald seed or at a short distance from the seed; they are associated with numerous tiny crystals that are in contact with the surface of the seed. Note also the distinctive color zoning in the seed. Immersion, magnified 80×.

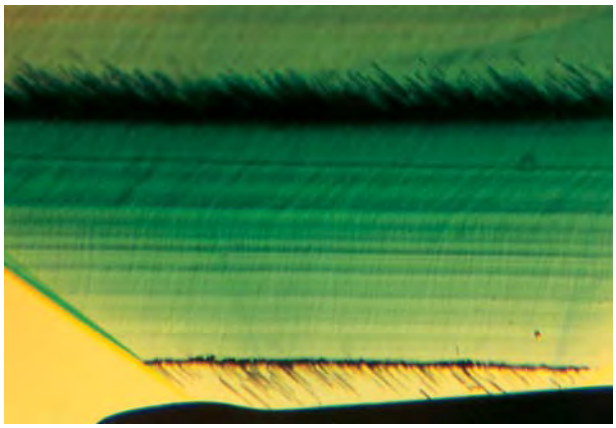

Identification of the Crystalline Inclusions. Tiny crystals at the base of nailhead spicules are common in hydrothermal synthetic emeralds (Pough, 1965; Flanigen et al., 1967; Galia, 1972; Sunagawa, 1982; Brown and Snow, 1984; Kane and Liddicoat, 1985; Gübelin, 1986; Hosaka, 1990; Hänni, 1993). They form when crystal growth starts on a seed plane that is inclined to the c-axis (Flanigen et al., 1967; Schmetzer, 1996). This type of inclusion also forms in flux-grown emerald (Flanigen et al., 1967), but it is commonly seen only in the Nacken products, which were grown in the 1920s on irregularly shaped seeds (Nassau, 1978).

On the basis of their R.I. (above that of beryl) and their crystal morphology, crystalline "nailheads" in hydrothermal synthetic emeralds are generally designated as phenakite (see references cited above). This identification was confirmed for Linde hydrothermal synthetic emerald by Raman spectroscopy (Delé-Dubois et al., 1986a and b). Examination of the inclusions in our Chinese samples, however, did not lead to the same results. Micro-Raman analysis of the birefringent crystals at the broad end of isolated spicules in samples B and E revealed only beryl. Thus, these inclusions are beryl crystals, but with an orientation different from that of the host. However, the Raman spectra of the numerous tiny crystallites that are also in contact with a seed (figure 15) did not match those of either beryl or phenakite; rather, they matched the spectrum of chrysoberyl (figure 16).

Examination of other hydrothermal synthetic emeralds (see Materials and Methods) proved the presence of phenakite in nailhead-type inclusions of several Linde and both types of Lechleitner synthetic emeralds. In the course of this study, with the help of Dr. Graham Brown in selecting the sample at the producer, "nailheads" of chrysoberyl crystals were identified for the first time at the seed of

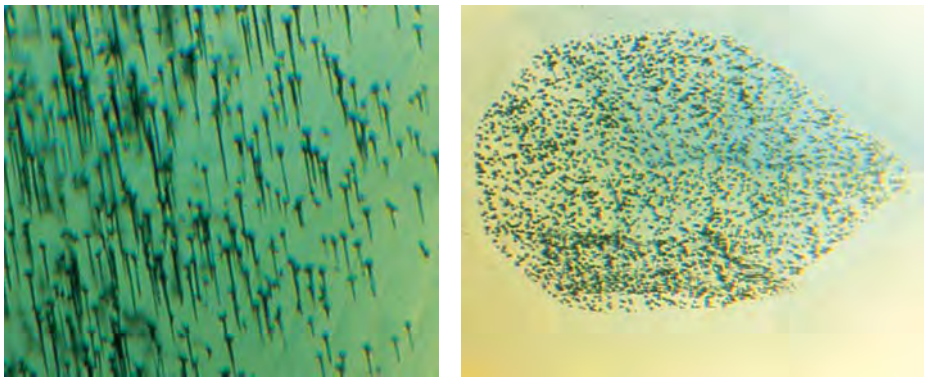

Figure 13. In the Chinese samples, the numerous tiny crystals at the broad ends of the spicules may appear as masses at the surface of the seed (left; immersion, magnified 50×). In a view parallel to the c-axis (i.e., the axis of the spicules), only the "nailheads" are visible; the cut of the synthetic emerald defines the outline of the seed (right; immersion, magnified 40×).

another hydrothermal synthetic emerald, the Biron product. Raman spectroscopy also identified some of the birefringent and transparent "nailheads" in two Biron synthetic emeralds as beryl, but found no phenakite in the samples analyzed. Interestingly, gold was also identified in these Biron samples; it probably originated from the liner of the autoclave, as indicated by the producer (A. Birkner, pers. comm., 1997) and by Kane and Liddicoat (1985).

Figure 14. The third type of elongated inclusion seen in the Chinese samples consists of needle-like tubes with an orientation almost perpendicular to the surface of the synthetic emerald seed (seen at the bottom here). On the other side of this boundary, in the synthetic emerald overgrowth, the cone-shaped spicules are elongated parallel to the c-axis. They start at the seed or at a short distance from the seed, and are often associated with tiny birefringent crystals that are in contact with the seed. (Note that the inclusion above the spicule on the right is not directly related to the spicule.) Immersion, crossed polarizers, magnified 80×.

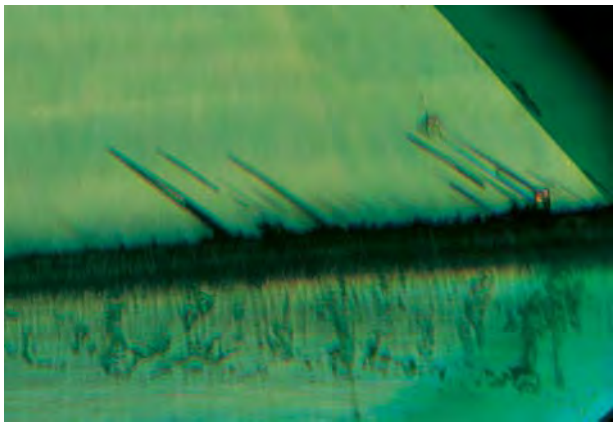

Chemistry. The qualitative EDXRF spectra of seven samples indicate distinct amounts of chromium and chlorine as well as the expected silicon and aluminum. Some minor vanadium was observed in one of the crystals.

Quantitative EDXRF and electron microprobe data are summarized in table 3. The microprobe data confirm the EDXRF results. The only color-causing element detected was chromium; vanadium and iron were at the detection limits of the electron microprobe. Alkalis and Mg were also at the detection limits, whereas significant amounts of chlorine and traces of fluorine were found in all samples.

Microprobe traverses indicated that chromium was the only element that varied appreciably from one area of a stone to another. This was most appar-

Figure 15. Micro-Raman analysis revealed that the tiny crystals at the broad ends of the numerous one- and two-phase cone-shaped spicules in the Chinese hydrothermal synthetic emeralds were chrysoberyl. Renishaw Raman microscope, magnified 200×.

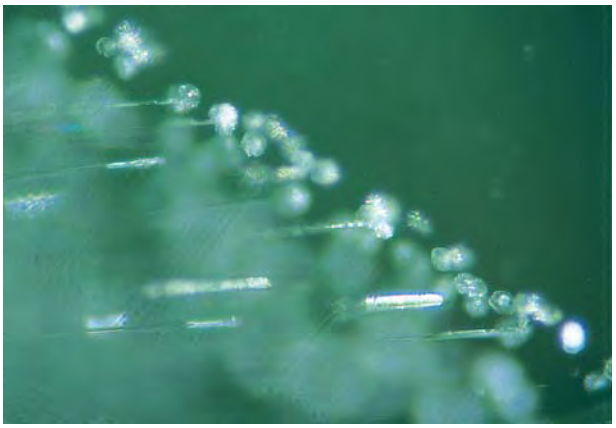

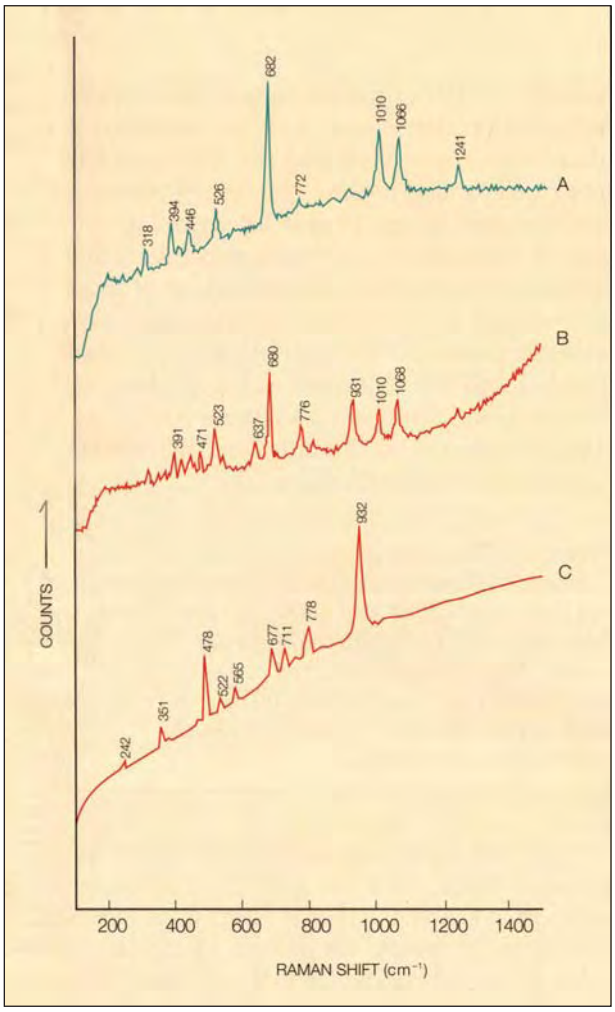

Figure 16. The Raman spectrum of the tiny crystals (B) illustrated in figure 15 match the reference spectrum for chrysoberyl (C). Note that in spectrum B, the lines of the Raman spectrum of the Chinese hydrothermal synthetic emerald host (A) are also present.

ent in samples C and F, where the traverses crossed the table facet, which included several different growth layers and color zones (figure 17).

Wet chemical analyses of sample F indicated a distinct water content of 0.85%, as well as the expected beryllium, but no lithium was found.

Spectroscopy. Because of the orientation of the samples, polarized spectra were measured only for two Chinese hydrothermal synthetic emerald crystals and one faceted sample. Nonpolarized spectra were recorded for four other faceted samples.

Ultraviolet-Visible Spectroscopy. The absorption spectra of all samples were consistent with the known absorption spectra of chromium in emerald; no absorption bands related to Fe^{2+} or Fe^{3+} were observed (for the exact position of iron absorption bands, see Schmetzer, 1988).

Infrared Spectroscopy. Infrared spectroscopy has been used to separate natural and synthetic emeralds since the late 1960s (Flanigen et al., 1967; Wood and Nassau, 1967, 1968; Nikol'skaya and Samoilovich, 1979; Klyakhin et al., 1981; Lebedev et al., 1986). With modern Fourier-transform infrared spectrometry, it is possible to obtain transmission and/or reflection infrared spectra on faceted samples (Flamini et al., 1983; Leung et al., 1986; Stockton, 1987; Fritsch et al., 1992; Hänni and Kiefert, 1994; Koivula et al., 1996).

The strongest absorption bands of at least two different types of water molecules located in channel sites of the beryl structure (both natural and synthetic) are found in the 3500–4000 cm^{-1} range of the mid-infrared. An extremely intense water absorption was observed in the spectra of the

TABLE 3. Chemical properties of Chinese hydrothermal synthetic emeralds.

Oxide (wt.%)	EDXRF (crystals)		Electron microprobe[a] (faceted stones)				
	A	B	C	D	E	F[b]	G
SiO_2			64.78	65.44	64.79	65.45	64.71
TiO_2			tr.[c]	tr.	tr.	tr.	tr.
Al_2O_3			18.37	18.66	18.25	18.46	18.39
Cr_2O_3	0.74	0.29	0.79	0.62	0.62	0.49	0.82
V_2O_3	n.d.[d]	0.03	tr.	tr.	tr.	tr.	tr.
FeO[e]	n.d.	n.d.	tr.	tr.	tr.	tr.	tr.
MnO			tr.	tr.	tr.	tr.	tr.
CaO			tr.	tr.	tr.	tr.	tr.
MgO			tr.	tr.	tr.	tr.	tr.
Na_2O			0.04	tr.	tr.	tr.	tr.
K_2O			tr.	tr.	tr.	tr.	tr.
F			0.04	0.04	0.03	0.04	0.04
Cl			0.67	0.71	0.65	0.69	0.67
Sum[f]			84.69	85.47	84.34	84.13	84.63
Cr_2O_3 (range)			0.39–1.08	0.54–0.71	0.54–0.73	0.27–0.60	0.69–1.07

[a] *Average of 100 point analyses.*
[b] *Wet chemical analysis gave 0.85 wt.% H_2O; Li_2O was not detected.*
[c] *tr.=trace (up to 0.02 wt.%).*
[d] *n.d.=not detected.*
[e] *Total iron is reported as FeO.*
[f] *BeO was calculated between 13.45 and 13.95 wt.% for the five samples, assuming 3.0 Be atoms per formula unit.*

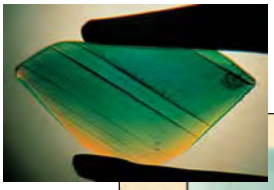

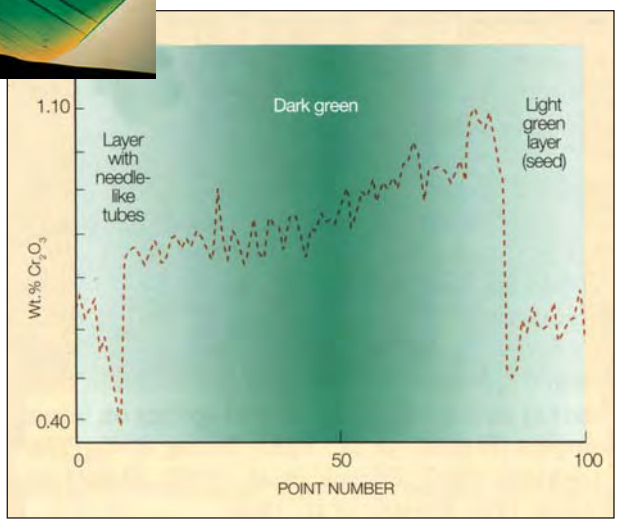

Figure 17. This graph shows the variation in Cr_2O_3 determined by electron microprobe analysis in a scan of 100 analytical points across the table facet (3 mm long) of sample C. Growth layers represented by color zoning in this sample (inset, in immersion, magnified 25×) are exposed at the table, as is the light green seed (on the right). Low levels of chromium are present in the seed, as compared to the remaining dark green area. The discontinuity on the left of this scan was measured at the boundary of another dark green area, close to a growth zone containing numerous needle-like tubes.

Chinese samples (figure 18). Between 5000 and 5500 cm^{-1} are absorption bands of other vibrations of water molecules. All different water absorption bands are strongly polarized (Wood and Nassau, 1968; Koivula et al., 1996), as we observed in the spectra of the Chinese samples.

In the 5000–5500 cm^{-1} region, it is possible to distinguish between the polarized spectra of alkali-free hydrothermal synthetic emeralds, such as our Chinese samples, and those of low-alkali natural emeralds, such as Colombian stones. The spectra must be recorded from oriented samples, because nonpolarized spectra of emeralds in the range of the water absorption bands are not always diagnostic (see Box A).

There is, however, another diagnostic range in the mid-infrared, between 2500 and 3100 cm^{-1}. All of our (chlorine-bearing) Chinese samples revealed a series of three sharp bands at 2746, 2815, and 2887 cm^{-1}, two broad absorption bands at about 2625 and 2970 cm^{-1}, and a smaller shoulder at 2917 cm^{-1} (figure 19). All five of the absorption bands are strongly polarization dependent: Four are polarized perpendicular to the c-axis, and the 2815 cm^{-1} band is polarized parallel to the c-axis. In nonpolarized spectra (compare figures 19 and 20), the relative intensities of these absorption bands depend on the orientations of the samples. A comparison of these spectra with those of other hydrothermal synthetic emeralds revealed an identical series of absorption bands in all the chlorine-bearing products—Linde, Regency, and Biron (see also figure 20 and Stockton, 1987)—but not in the chlorine-free Russian and Lechleitner synthetic emeralds.

Figure 18. The infrared spectra of faceted Chinese hydrothermal synthetic emerald sample C between 2000 and 6000 cm^{-1} are shown here polarized perpendicular and parallel to the c-axis. Note the water-related peaks in the 3500–4000 cm^{-1} and 5000–5500 cm^{-1} regions, as well as the chlorine-related peaks in the 2500–3100 cm^{-1} region.

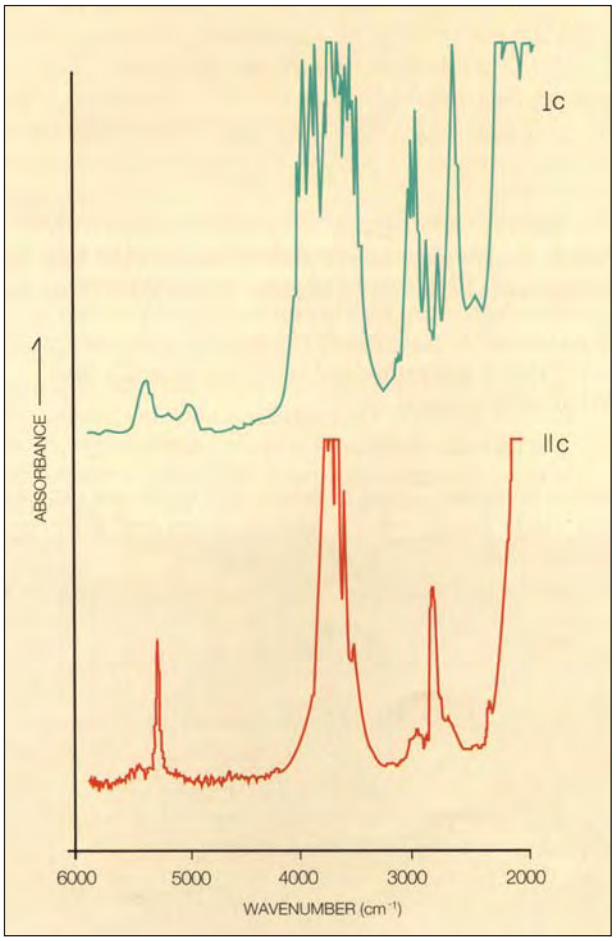

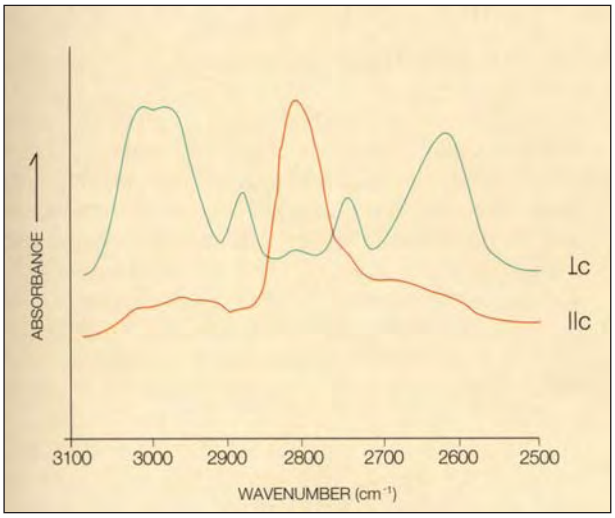

Figure 19. Chlorine-related bands in the 2500–3100 cm^{-1} range of the infrared spectrum, as seen polarized parallel and perpendicular to the c-axis, are diagnostic for the Chinese and other chlorine-bearing hydrothermal synthetic emeralds.

This group of bands is probably related to the chlorine content of these samples. Observation of this series of absorption bands in an unknown sample is sufficient to identify the sample as synthetic; no overlap with any absorption bands seen in natural emeralds is found in the 2500–3100 cm^{-1} range. In addition, polarized spectra are not needed; that is, a sample does not need to be oriented to obtain diagnostic information in this range.

DISCUSSION

Growth Conditions of Chinese Hydrothermal Synthetic Emeralds. The results of our study indicate that Chinese hydrothermal synthetic emeralds belong to the group of chlorine-bearing, alkali-free hydrothermal emeralds that includes two types of products: (1) Linde and Regency (predominantly Cr-bearing); and (2) Biron, Pool, and AGEE (predominantly Cr- and V-bearing). The other group of hydrothermal synthetic emeralds—those that are alkali-bearing and chlorine-free—includes the Lechleitner products and all commercial Russian hydrothermal synthetic emeralds. Samples of the alkali-free group reveal infrared absorption bands of type I water molecules only, whereas samples of the alkali-containing group show bands related to type I and type II water (again, see Box A).

Those Chinese samples that contain a colorless natural seed were grown in a single production step. Those that consist of a green synthetic seed with an overgrowth of synthetic emerald represent two generations of growth: A plate of synthetic emerald was cut from a previously grown crystal, and this plate was used as a seed to grow layers of a second generation (as confirmed by E. Fritsch, pers. comm., 1997, and C. M. Ou-Yang, pers. comm., 1997). This is similar to the procedure used to grow the first hydrothermal synthetic emeralds, such as Lechleitner and Linde, in several subsequent autoclave runs. The morphology of the crystals is dominated by the orientation and size of the seed, especially the relationship of length to width (again, see figure 3).

Samples A and H, which were obtained in 1994 and 1995, respectively, and show irregular growth faces parallel to the seed, probably represent an older type of Chinese synthetic emerald grown with a seed inclined 20° to the optic axis. All other samples were grown with seeds inclined 32° to 40° to the c-axis. According to the producer, he tried to cut the natural beryl plates used as seeds for the first growth step with an orientation of 30° to 35° to the c-axis. However, because of the properties of the natural beryl crystals that were available, he encountered problems orienting them, which

Figure 20. For Biron and Chinese hydrothermal synthetic emeralds in the 2500 and 3100 cm^{-1} range, the relative intensities of the bands seen with polarized spectra (figure 19) are different from those seen here with nonpolarized spectra.

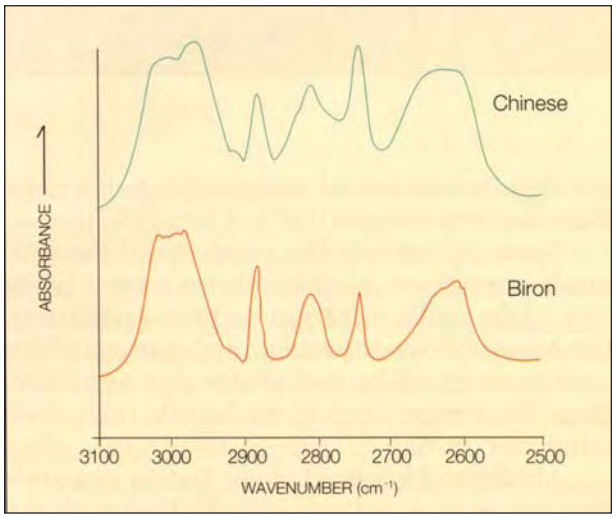

Box A: Distinction of Natural and Synthetic Emeralds by Water Absorption Bands in the Infrared

All natural and hydrothermal synthetic emeralds contain water in the relatively large channels inherent to the structure of beryl. Wood and Nassau (1968) identified two types of water molecules in beryl, as evidenced by absorption features in their infrared spectra. Type I water occurs in low-alkali natural and all hydrothermal synthetic emeralds. Type II water occurs in all alkali-bearing natural emeralds and some hydrothermal synthetic emeralds. Because of the presence of similar amounts of type I and type II water molecules, the absorption spectra of low-alkali hydrothermal synthetic emeralds (Russian samples and Lechleitner fully synthetic emeralds) overlap those of low-alkali natural emeralds such as from Colombia or Zimbabwe (Sandawana) in the 3500–4000 cm^{-1} range. Consequently, only high-alkali natural emeralds without type I water can be easily identified by their infrared spectra in that range (Schmetzer, 1988, 1989, 1990; Kiefert and Schmetzer, 1990).

Because of the high water contents of natural and hydrothermal synthetic emeralds, it is somewhat problematic to obtain the fine structure and exact positions of the absorption maxima of the water-related infrared absorption bands in the 3500–4000 cm^{-1} region from relatively thick crystals or from faceted stones (see text figure 18). The polarized measurement of spectra cannot solve this problem.

The information can be gained by obtaining a small amount of emerald powder (e.g., 2 mg) to prepare a KBr compressed disk, but this is a destructive method that is useful only in a research environment (Flanigen et al., 1967; Schmetzer, 1989; Schmetzer and Kiefert, 1990; Aurisicchio et al., 1994). Nevertheless, to fully characterize the Chinese hydrothermal synthetic emeralds, we obtained such data from sample F, which revealed a single sharp absorption band at 3964 cm^{-1}. This absorption band has been assigned to alkali-free (type I) water molecules in beryl (Wood and Nassau, 1968; Schmetzer, 1989). It is consistent with the chemical composition of sample F (see text table 3), which did not contain significant alkalis.

Even when the diagnostic absorptions in the 3500–4000 cm^{-1} region are too strong to be distinguishable, features in the 5000–5500 cm^{-1} region can usually be resolved. They are, therefore, particularly useful in the separation of natural from hydrothermal synthetic emeralds. In this region, other water vibrations were noted for seven Chinese samples: three distinct absorption maxima, at 5110, 5275, and 5450 cm^{-1}. All three absorption bands can also be assigned to alkali-free (type I) water molecules (Wood and Nassau, 1967, 1968, Nassau and Nassau, 1980; Klyakhin et al., 1981; Kodaira et al., 1982; Flamini et al., 1983; Lebedev et al., 1986; Koivula et al., 1996). This is consistent with the result obtained for sample F using the KBr technique. In some of the spectra obtained by conventional means, the 5275 cm^{-1} absorption band was dominant; in others, the three absorption bands were of similar intensity (figure A-1). The nonpolarized spectra of all seven samples lie between these two basic types, depending on the angle of the beam to the c-axis. However, the polarized spectra of three Chinese samples (figure A-2) revealed that the absorption bands at 5110 and 5450 cm^{-1} are polarized *perpendicular* to the c-axis and the band at 5275 cm^{-1} is polarized *parallel* to the c-axis. This polarization dependency is responsible for the variation in nonpolarized spectra according to the orientation of the sample.

resulted in a variety of angles within this range (Guo Tao, pers. comm., 1997).

Seeds inclined to the c-axis more than 35° result in synthetic emeralds that are more-or-less free of irregular internal growth structures. Consequently, the internal growth pattern of this product is similar to that observed in samples of recent Russian production (see Koivula et al., 1996; Schmetzer, 1996).

Although chrysoberyl is not known as a common inclusion in synthetic emerald, Flanigen (1971) mentioned that the formation of impurities such as chrysoberyl and phenakite had been observed during the growth of hydrothermal synthetic beryl. The hydrothermal synthesis of chrysoberyl is also described in the literature in the pressure-temperature range claimed by the producer for these Chinese hydrothermal synthetic emeralds (see, e.g., Franz and Morteani, 1981; Barton, 1986).

The results of our chemical analyses indicated two types of Chinese hydrothermal synthetic emeralds in our study: Most of the samples contained

It is important to note that alkali-bearing natural emeralds exhibit a type II water absorption band at 5275 cm^{-1} with polarization *perpendicular* to the c-axis (Wood and Nassau, 1967, 1968). Similar spectra have been reported for alkali-bearing hydrothermal synthetic emeralds from Russia and for low- to medium-alkali natural emeralds (Klyakhin et al., 1981; Flamini et al., 1983; Lebedev et al., 1986; Koivula et al., 1996). Because of the polarization differences (see figure A-2), it is possible to distinguish between type I and type II water spectra in the 5000–5500 cm^{-1} region.

However, *nonpolarized* spectra of low-alkali natural and synthetic emeralds are almost identical to those of alkali-free synthetic emeralds (again, see figure A-1). Consequently, nonpolarized absorption spectra in the 5000 to 5500 cm^{-1} region are of no diagnostic value. Only moderate- to high-alkali natural emeralds can be identified as natural on the basis of nonpolarized near-IR spectra in which type I absorption bands are absent.

Figure A-1. These nonpolarized infrared spectra of a Chinese hydrothermal synthetic emerald between 5000 and 5500 cm^{-1} were taken in a direction more or less perpendicular to the c-axis (A) and slightly oblique to the c-axis (B). They illustrate how the three main bands—at 5110, 5275, and 5450 cm^{-1}—can vary in intensity depending on the orientation of the sample.

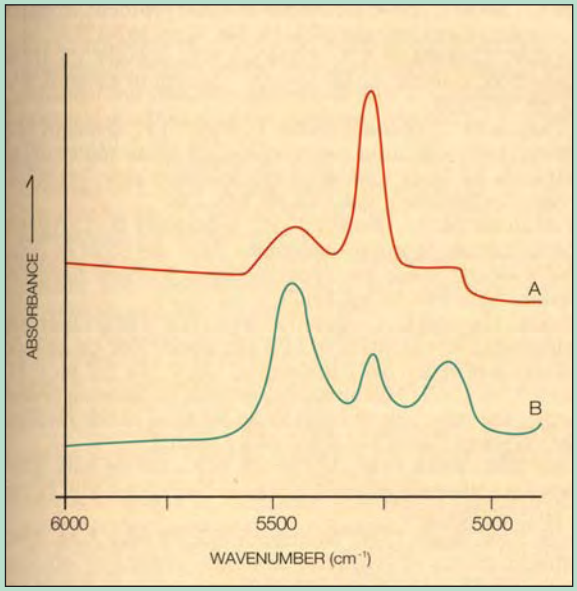

Figure A-2. In these polarized infrared spectra of Chinese hydrothermal synthetic emeralds in the 5000–5500 cm^{-1} region, the band at 5275 cm^{-1} is seen only when the beam is polarized parallel to the c-axis, whereas the bands at 5110 and 5450 cm^{-1} are seen only in spectra polarized perpendicular to the c-axis.

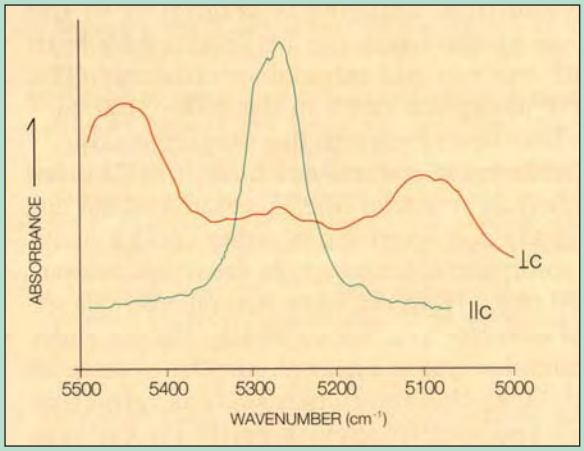

only chromium as the chromophore, but one specimen (sample B) also had small amounts of vanadium. The vanadium-containing specimen may represent the second type of earlier production described by the producer (see Background), but there was no iron present in the specimen we analyzed.

DIAGNOSTIC PROPERTIES

A new type of synthetic emerald is being produced in China by the hydrothermal method. Some of its characteristic properties, such as the use of natural or synthetic seeds, the orientation of seeds and growth planes, as well as a diagnostic chlorine content and the absence of alkalis, are consistent with those known for hydrothermal synthetic emeralds from other producers (e.g., Linde, Biron). Other characteristic features, such as the presence of tiny chrysoberyl crystals on the seeds, have only been identified in Biron hydrothermal synthetic emeralds (as described in this article).

Most of the samples examined revealed microscopic features of diagnostic value, including natu-

ral or synthetic seeds and a characteristic growth zoning parallel to the seed. The characteristic zoning forms an angle to the c-axis of the synthetic emerald, which can be determined easily with a horizontal microscope. This particular angle is diagnostic because no crystal faces of natural beryl are in this range—that is, between 20° and 40° to the c-axis. In addition, the irregular growth pattern characteristic of hydrothermal synthetic beryl was also found in some of the samples examined.

Spicules oriented parallel to the c-axis, commonly associated with tiny chrysoberyl or, rarely, beryl crystals at their widest ends are characteristic for Chinese hydrothermal synthetic emeralds and have not been reported in natural emeralds. The solid inclusions are related to the boundaries between the seed (natural colorless beryl or synthetic emerald) and the synthetic emerald. Needle-like tubes oriented almost perpendicular to the seed or to dominant growth faces are also characteristic for Chinese hydrothermal synthetic emeralds.

In addition, chlorine is diagnostic of the Chinese product and can be detected by both EDXRF analysis and infrared spectroscopy. The series of absorption bands in the 2500–3100 cm^{-1} region have never been seen in natural emeralds.

Unlike most natural emeralds, the Chinese hydrothermal synthetic emeralds examined did not contain any iron detectable by either EDXRF analysis or absorption spectroscopy in the visible to near-infrared range. However, some natural emeralds are almost iron-free and, consequently, do not show any iron absorption bands. A similar overlap of gemological characteristics such as refractive indices and specific gravity exists for Chinese hydrothermal synthetic emeralds and low-alkali natural emeralds from various localities.

Acknowledgments: The authors are grateful to Mrs. Guo Tao, Beijing, and Mrs. C. M. Ou-Yang, Hong Kong, China, for providing information about the producer and production techniques. Mr. B. Bruder, SSEF, Basel, Switzerland, and Dr. T. Häger, University of Mainz, Germany, are kindly acknowledged for their help with spectroscopy. Dr. O. Medenbach, Ruhr University, Bochum, Germany, performed goniometric measurements of the rough crystals. Hydrothermal synthetic emeralds from different producers, which were used for comparative studies, were submitted by A. Birkner, Biron Corp., Balcatta, Australia; Dr. G. Brown, Brisbane, Australia; W. Galia, Bergisch Gladbach, Germany; Prof. E. Gübelin, Lucerne, Switzerland; Prof. H. A. Hänni, SSEF, Basel, Switzerland; and F.-J. Schupp, Pforzheim, Germany. Discussions with Prof. E. Fritsch, University of Nantes, France, were very helpful in finalizing this article.

REFERENCES

Aurisicchio C., Grubessi O., Zecchini P. (1994) Infrared spectroscopy and crystal chemistry of the beryl group. *Canadian Mineralogist*, Vol. 32, pp. 55–68.

Barton M.D. (1986) Phase equilibria and thermodynamic properties of minerals in the BeO-Al_2O_3-SiO_2-H_2O (BASH) system, with petrologic applications. *American Mineralogist*, Vol. 71, No. 3/4, pp. 277–300.

Brown G., Snow J. (1984) Inclusions in Biron synthetic emeralds. *Australian Gemmologist*, Vol. 15, No. 5, pp. 167–171.

Bukin G.V., Godovikov A.A., Klyakhin V.A., Sobolev V.S. (1986) Growth of emerald single crystals. *Growth of Crystals*, Vol. 13, pp. 251–260.

Delé-Dubois M.L., Dhamelincourt P., Poirot J.P., Schubnel H.-J. (1986a) Differentiation between natural gems and synthetic minerals by laser Raman micro-spectrometry. *Journal of Molecular Structure*, Vol. 143, pp. 135–138.

Delé-Dubois M.-L., Poirot J.-P., Schubnel H.-J. (1986b) Identification de micro-inclusions dans des rubis et émeraudes de synthèse par spectroscopie Raman. *Revue de Gemmologie*, No. 88, pp. 15–17.

Flamini A., Gastaldi L., Grubessi O., Viticoli S. (1983) Contributo della spettroscopia ottica ed EPR alla distinzione tra smeraldi naturali e sintetici. *La Gemmologia*, Vol. 9, No. 1/2, pp. 6–11.

Flanigen E.M. (1971) Hydrothermal process for growing crystals having the structure of beryl in an alkaline halide medium. United States Patent No. 3,567,642; March 2.

Flanigen E.M., Breck D.W., Mumbach N.R., Taylor A.M. (1965) New hydrothermal emerald. *Gems & Gemology*, Vol. 11, No. 9, pp. 259–264, 286.

Flanigen E.M., Breck D.W., Mumbach N.R., Taylor A.M. (1967) Characteristics of synthetic emeralds. *American Mineralogist*, Vol. 52, No. 5/6, pp. 744–772.

Franz G., Morteani G. (1981) The system BeO-Al_2O_3-SiO_2-H_2O: Hydrothermal investigation of the stability of beryl and euclase in the range from 1 to 6 kb and 400 to 800°C. *Neues Jahrbuch für Mineralogie Abhandlungen*, Vol. 140, No. 3, pp. 273–299.

Fritsch E. (1996) Chinese synthetics: The anonymous crowd. *Jewelers' Circular-Keystone*, Vol. 167, No. 3, pp. 51–52.

Fritsch E., Muhlmeister S., Birkner A. (1992) A preliminary study of the Biron synthetic pink titanium-beryl. *Australian Gemmologist*, Vol. 18, No. 3, pp. 81–82.

Galia W. (1972) Diagnostische Merkmale Synthetischer smaragde von Linde. *Zeitschrift der Deutschen Gemmologischen Gesellschaftt*, Vol. 21, No. 2, pp. 112–117.

Geng G.L., Ou-Yang C.M. (1995) How to indentify hydrothermal synthetic emerald from China. *Jewellery News Asia*, No. 130, p. 92, 94.

Gübelin E. (1986) Die diagnostischen Eigenschaften der neuesten Synthesen. *Goldschmiede und Uhrmacher Zeitung*, Vol. 84,

No. 11, pp. 69–76.
Hänni H.A. (1993) Hydrothermalsynthesen aus Australien: smaragd und rosaberyll. *Swiss Jewelry and Watchmaker Journal*, April 1993, pp. 45–48.
Hänni H.A., Kiefert L. (1994) AGEE hydrothermal synthetic emeralds. *JewelSiam*, Vol. 5, No. 5, pp. 80–85.
Hänni H.A., Kiefert L., Chalain J.-P., Wilcock I.C. (1996) Ein Renishaw Raman Mikroskop im gemmologischen Labor: Erste Erfahrungen bei der Anwendung. *Zeitschrift der Deutschen Gemmologischen Gesellschaft*, Vol. 45, No. 2, pp. 55–69.
Hänni H.A., Kiefert L., Chalain J.-P., Wilcock I.C. (1997) A Raman microscope in the gemmological laboratory: First experiences of application. *Journal of Gemmology*, Vol. 25, No. 6, pp. 394–406.
Henn U., Lind T., Bank H. (1988) Hydrothermal grown synthetic emeralds from USSR. *Canadian Gemmologist*, Vol. 9, No. 3, pp. 66–72.
Hosaka M. (1990) Hydrothermal growth of gem stones and their characterization. *Progress of Crystal Growth and Characterization*, Vol. 21, pp. 71–96.
Kane R.E., Liddicoat R.T. Jr. (1985) The Biron hydrothermal synthetic emerald. *Gems & Gemology*, Vol. 21, No. 3, pp. 156–170.
Kiefert L., Schmetzer K. (1991) The microscopic determination of structural properties for the characterization of optical uniaxial natural and synthetic gemstones. Part 1: General considerations and description of the methods. *Journal of Gemmology*, Vol. 22, No. 6, pp. 344–354.
Klyakhin V.A., Lebedev A.S., Il'in A.G., Solntsev V.P. (1981) Growing of hydrothermal beryl (in Russian). In *Sintez i Vyrashchivanie Optich*. Kristallov i Yuvelir. Kamnei, Novosibirsk, pp. 45–66.
Kodaira K., Iwase A., Tsunashima A., Matsushita T. (1982) High-pressure hydrothermal synthesis of beryl crystals. *Journal of Crystal Growth*, Vol. 60, pp. 172–174.
Koivula J.I., Kammerling R.C., DeGhionno D., Reinitz I., Fritsch E., Johnson M.L. (1996) Gemological investigation of a new type of Russian hydrothermal synthetic emerald. *Gems & Gemology*, Vol. 32, No. 1, pp. 32–39.
Lebedev A.S., Askhabov A.M. (1984) Regeneration of beryl crystals (in Russian). *Zapiski Vsesoyoznogo Mineralogicheskogo Obshchestva*, Vol. 113, No. 5, pp. 618–628.
Lebedev A.S., Il'in A.G., Klyakhin V.A. (1986) Hydrothermally grown beryls of gem quality (in Russian). In *Morphology and Phase Equilibria of Minerals. Proceedings of the 13th General Meeting of the International Mineralogical Association, Varna 1982*, Vol. 2, Sofia, Bulgaria, pp. 403–411.
Leung C.S., Merigoux H., Poirot J.P., Zecchini P. (1986) Use of infrared spectrometry in gemmology. In *Morphology and Phase Equilibria of Minerals. Proceedings of the 13th General Meeting of the International Mineralogical Association, Varna 1982*, Vol. 2, Sofia, Bulgaria, pp. 441–448.
Nassau K. (1976) Synthetic emerald: The confusing history and the current technologies. *Journal of Crystal Growth*, Vol. 35, pp. 211–222.
Nassau K. (1978) Did Professor Nacken ever grow hydrothermal emerald? *Journal of Gemmology*, Vol. 16, No. 1, pp. 36–49.
Nassau K., Nassau J. (1980) The growth of synthetic and imitation gems. In Freyhart H.C., Ed., *Crystals: Growth Properties and Applications*, Vol. 2, Springer, Berlin, pp. 1–50.
Nikol'skaya L.V., Samoilovich M.I. (1979) Optical absorption spectra of beryls in the near infrared (900–2500 nm). *Soviet Physics-Crystallography*, Vol. 24, No. 5, pp. 604–606.
Pough F.H. (1965) A new hydrothermal synthetic emerald. *Journal of Gemmology*, Vol. 9, No. 12, pp. 426–433.
Schmetzer K. (1986) An improved sample holder and its use in the distinction of natural and synthetic ruby as well as natural and synthetic amethyst. *Journal of Gemmology*, Vol. 20, No. 1, pp. 20–33.
Schmetzer K. (1988) Characterization of Russian hydrothermally grown synthetic emeralds. *Journal of Gemmology*, Vol. 21, No. 3, pp. 145–164.
Schmetzer K. (1989) Types of water in natural and synthetic emerald. *Neues Jahrbuch für Mineralogie Monatshefte*, Vol. 1989, No. 1, pp. 15–26.
Schmetzer K. (1990) Two remarkable Lechleitner synthetic emeralds. *Journal of Gemmology*, Vol. 22, No. 1, pp. 20–32.
Schmetzer K. (1996) Growth method and growth-related properties of a new type of Russian hydrothermal synthetic emerald. *Gems & Gemology*, Vol. 32, No. 1, pp. 40–43.
Schmetzer K., Kiefert L. (1990) Water in beryl: A contribution to the separability of natural and synthetic emeralds by infrared spectroscopy. *Journal of Gemmology*, Vol. 22, No. 4, pp. 215–223.
Schrader H.-W. (1983) Contributions to the study of the distinction of natural and synthetic emeralds. *Journal of Gemmology*, Vol. 18, No. 6, pp. 530–543.
Sechos B. (1997) Identifying characteristics of hydrothermal synthetics. *Australian Gemmologist*, Vol. 19, No. 9, pp. 383–388.
Sosso F., Piacenza B. (1995) Russian hydrothermal synthetic emeralds: Characterization of the inclusions. *Journal of Gemmology*, Vol. 24, No. 7, pp. 501–507.
Stockton C.M. (1987) The separation of natural from synthetic emeralds by infrared spectroscopy. *Gems & Gemology*, Vol. 23, No. 2, pp. 96–99.
Sunagawa I. (1982) Gem materials, natural and artificial. In Kaldis E., Ed., *Current Topics in Materials Science*. Vol. 10, North-Holland Publishing Company, Amsterdam, pp. 353–497.
Wood D.L., Nassau K. (1967) Infrared spectra of foreign molecules in beryl. *Journal of Chemical Physics*, Vol. 47, No. 7, pp. 2220–2228.
Wood D.L., Nassau K. (1968) The characterization of beryl and emerald by visible and infrared absorption spectroscopy. *American Mineralogist*, Vol. 53, No. 5/6, pp. 777–800.